Enhanced removal of Indigo Carmine dye from textile effluent using green cost-efficient nanomaterial: Adsorption, kinetics, thermodynamics and mechanisms

Mai El-Kammah [a], Elsayed Elkhatib [b], Susana Gouveia [c], Claudio Cameselle [c,*], Emad Aboukila [a]

[a] *Department of Natural Resources and Agricultural Engineering, Faculty of Agriculture, Damanhour University, Damanhour, 22511, Egypt*
[b] *Department of Soil and Water Sciences, Faculty of Agriculture (El-Shatby), Alexandria University, Alexandria, 21545, Egypt*
[c] *University of Vigo, BiotecnIA Group, Department of Chemical Engineering, 36310, Vigo, Spain*

ABSTRACT

The release of Indigo Carmine in waterbodies may cause serious impact in aquatic ecosystems and human health. There is an interest in developing green, low-cost and effective adsorbents for the removal of toxic dyes from textile effluents. This study proposed the developing of an adsorbent material at the nanoscale using the waste from *Moringa oleifera* seeds generated after the oil extraction. *Moringa oleifera* seeds were grounded to obtain an adsorbent material at the nanoscale. Batch-adsorption tests were carried out to evaluate the capacity of the absorbent to retain Indigo Carmine from liquid solutions. The following variables were studied: pH, adsorbent-dye ratio, contact time, initial dye concentration and temperature. The adsorption process fitted the Langmuir isotherm in the equilibrium of adsorption and the power function in the kinetic behavior. The maximum adsorption capacity of the absorbent nanoparticles was 60.24 mg/g, which is 4.3 times higher than that of the bulk *Moringa oleifera* seeds. Thermodynamic results proved the adsorption process was spontaneous and exothermic. Hydrogen bonding, electrostatic interlinkage and π–π interactions were identified as the dominant mechanisms of Indigo Carmine adsorption on the nanoparticles. The adsorption-desorption study resulted in a slight decrease of the adsorption capacity after 4 cycles, from 94% to 88%. The removal of Indigo Carmine from a textile effluent (85%) was similar to that with pure Indigo Carmine solutions (91%). The results suggested the feasibility of *Moringa oleifera* seed nanoparticles as a promising, green and low cost adsorbent for textile wastewaters with dyes.

1. Introduction

Dyes are common and critical components in the wastewaters from textile industry. Indigo carmine (IC) is a dye and colorant with applications in the pharmaceutical, textile, leather and food industries (Tabti et al., 2022). Besides, IC is also used as redox indicator in analytical chemistry (Edwin et al., 2021) and photometric detector (Gokul Eswaran et al., 2022). In the textile industry, IC is widely used in the dyeing of denim (Choi, 2021). Considering its frequent usage and toxic effects in aquatic ecosystems, IC is considered a

contaminant to be treated and/or removed before the discharge of wastewaters in the environment (Behera et al., 2021).

The treatment and removal of dyes from textile wastewater involved various physicochemical and biological technologies, including membrane separation, chemical precipitation, adsorption, electrochemical degradation, advanced oxidation processes and others (Donkadokula et al., 2020; Behera et al., 2021). However, most of those technologies are expensive due to the consumption of energy and chemicals, and often, the treatment is inefficient (Ramos et al., 2021). One economic and promising option is the use of adsorption processes based on waste materials as adsorbents (Afroze and Sen, 2018; Sikdar et al., 2020). The ready availability of lignocellulosic materials and its very low cost made such materials the best candidates for developing sustainable adsorption processes (Chowdhury et al., 2020). Numerous lignocellulosic materials were tested for the adsorption of dyes from aqueous solutions with moderately successful results (Shirani et al., 2018; Wakkel et al., 2019; Chowdhury et al., 2020; Sikdar et al., 2020). The development of practical adsorption process at industrial scale requires fast and complete adsorption of the dye contaminants from wastewater. It is also important the desorption of the contaminant and the reuse of the adsorbent. However, considering the low cost of the lignocellulosic materials, the reusability is not a critical aspect in the developing of the adsorption process. Several researchers have suggested modification in the adsorbent with the objective to increase the adsorption capacity and kinetics. Zein et al. (2022) combined *Terminalia catappa* shell and egg white to reach a maximum adsorption capacity of 107 mg/g for Indigo Carmine. Du et al. (2022) chemically modified kapok fiber to insert functional groups that enhanced the adsorption selectivity and capacity (129 mg/g) of Indigo Carmine. Carbon composites and activated carbon derived from lignocellulosic and other organic waste materials is another approach to obtain highly active adsorbent at low cost (Davies and McGregor, 2021).

Another alternative method to enhance the adsorption capacity of an adsorbent is the preparation of nanoparticles. The properties of the nanoparticles are rather different from the bulk material. At the nanoscale, materials may show new and unexpected properties, different from those at the macroscale (Cameselle and Reddy, 2019). In adsorbent materials, the adsorption capacity and reactivity is enhanced due to the large ratio surface/volume at the nanoscale compared with the bulk material (Elkhatib et al., 2017; El-Kammah et al. 2022). Thus, replacing the costly commercial nanomaterials by cheap nanoscale sorbents derived from lignocellulosic bio-waste has been proposed as a practical and sustainable alternative to develop adsorption processes at large scale.

Wasted biomass from *Moringa oleifera* has been tested as an inexpensive absorbent material for various contaminants in aqueous effluents, including IC. Agbahoungbata et al. (2016) have tested *M. oleifera* seeds for the adsorption of IC, suggesting that it could be an interesting adsorbent material. Other authors have used *M. oleifera* biomass to prepare various adsorbents o coagulants for the removal of Indigo Carmine and other contaminants (Gomes et al., 2022). El-Kammah et al. (2022a, b) have tested nanosized absorbent materials prepared from wastes for the removal of IC and thyametoxam pesticide. In this study, we hypothesized that the adsorption capacity of *M. oleifera* seeds could be enhanced preparing a nanosized absorbent material as described by El-Kammah et al. (2022a, b). So, we pursued to developed an inexpensive adsorbent materials derived from wasted biomass with an enhanced adsorption capacity.

The objectives of this study are: a) prepare an adsorbent material at the nanoscale from the by-products of *Moringa oleifera* oil production, b) test the adsorption capacity of the nanosorbent with the dye Indigo Carmine using pure solutions and textile wastewaters, c) determine the operational conditions of Indigo carmine adsorption through a series of adsorption, kinetic and thermodynamic studies, and d) assess the stability and reusability of the nanosorbent derived from *Moringa oleifera* seeds.

2. Materials and methods

2.1. Adsorbent material from Moringa oleifera seeds

Moringa oleifera seeds (MOS) were obtained from the department of agriculture in Cairo, Egypt. *Moringa oleifera* was cultivated to obtain essential oil from its seeds, based on a solvent extraction process (Anwar et al., 2005). After the extraction process, the oil-free press cake was oven dried at 60 °C to ensure the complete volatilization of the solvent. The dried cake was sieved through 2 mm and 51 μm mesh. The fraction that passed through the 2 mm mesh was identified as bulk *Moringa oleifera* seeds (bMOS). The fraction that passed through the 51 μm mesh was grounded in a ball mill (Fritsch, Germany) to produce nanoscale particles (nMOS) with a particle size below 100 nm following the method described by Elkhatib et al. (2015). X-Ray Diffraction (XRD) and transmission electron microscopy (TEM) analyses of nMOS are reported in supplementary material (Section 1, Figs. S1 and S2).

2.2. Characterization of adsorbent materials

The morphology, nature and the elemental composition of the two adsorbent materials: nMOS and bMOS, were determined by SEM-EDS (Scanning Electron Microscopy-Energy Dispersive Spectroscopy) using a JSM-IT200 Series apparatus (Oxford Instruments), and FTIR spectroscopy (Fourier-transform infrared spectroscopy) using a Perkin Elmer Model 400 apparatus. The point of zero charge (pH_{PZC}) of nMOS was determined with the method described by Kosmulski (2009). nMOS specimens of 0.20 g were suspended in 50 mL of 0.01 M NaCl solution in volumetric flasks at various pH in the range from pH = 2 to pH = 11. The pH of the nMOS suspensions was adjusted using HCl/NaOH solutions. The suspension was shaken for 1 h and the final pH of each suspension was recorded. pH_{PZC} was determined plotting the difference between the initial and final pH versus the initial pH for each suspension. The intersection point of the resulting curve with the horizontal axis is the pH_{PZC}. bMOS and nMOS specific surface area were determined with a surface area analyzer from Quantachrome (USA).

2.3. Indigo Carmine

Indigo Carmine (IC) pure solutions prepared in the laboratory with deionized water were used as adsorbate to test the absorption capacity of nMOS and bMOS. IC analytical reagent grade, with purity >99%, was purchased from ANALEMA (Vigo, Spain). IC dye stock solution of 1000 mg/L was prepared using deionized water. All working solutions for the adsorption tests were freshly prepared

daily by diluting the IC stock solution. IC concentration in water solutions before and after the adsorption tests was determined at 610 nm using a UV–Vis spectrophotometer (model GENESYS 10S, Fisher Scientific). The straight line for the calibration of the absorbance at 610 nm and the IC concentration was determined in the range 0–100 mg/L. Samples with IC concentration higher than 100 mg/L were diluted with deionized water before analysis. Characteristics and chemical structure of IC dye are reported in the supplementary material (Section 2, Fig. S3).

2.4. Adsorption tests

The adsorption tests of IC on bMOS and nMOS were performed by mixing 0.1 g of adsorbent with 40 mL of IC solution. The mixtures were shaken at 160 rpm and 25 °C for a maximum of 24 h. At the end of the tests, the suspensions were centrifuged at 4000 rpm (1800 g) for 5 min and the supernatant was filtered through a 0.45 μm membrane filter (Millipore). The IC concentration in the supernatant was determined by UV–Vis spectrophotometry at 610 nm.

IC removal from the aqueous solutions in the adsorption tests was calculated with equation (1).

$$\text{IC removal (\%)} = ((C_0 - C_e) / C_0) \cdot 100 \qquad [1]$$

Where C_0 is the initial concentration of IC in the liquid phase in mg/L, C_e is the IC concentration at the end of the test in the liquid phase in equilibrium with the solid phase (adsorbent) in mg/L.

The adsorption capacity (q_e) of the absorbent in equilibrium with the liquid phase was calculated using equation (2).

$$q_e \text{ (mg/g)} = (C_0 - C_e) \cdot V / m \qquad [2]$$

Where V is the volume of the liquid phase expressed in L, and m is the adsorbent mass expressed in g. The adsorption experimental results were modeled using six adsorption isotherms (Table 1) and four kinetic models (Table 2).

Various adsorption tests of IC on nMOS were designed and conducted to determine the influence of contact time (5–120 min), IC solution pH (pH = 2–11), nMOS adsorbent dose (0.1–0.4 g), temperature (298.15–318.15 K) and IC initial concentration (10–400 mg/L), in the adsorption equilibrium, adsorption kinetics and thermodynamic behavior.

The adsorption capacity of nMOS for IC in textile wastewater was tested in batch and packed-bed column. The batch tests were carried out mixing 0.2 g of adsorbent (nMOS) with 80 mL of textile wastewater (43.65 mg/L of IC), or IC pure solution (50 mg/L), for 40 min. The packed–bed column system was set up using a Pyrex column (30 cm long and 2.5 cm in diameter). A 10 cm supporting layer of gravel was placed in the bottom of the column with a very fine wire mesh covered with cellulose filter paper to avoid any loss of the solid material. The column was filled with 200 mg of nMOS mixed with a portion of fine and coarse sand. The textile wastewater (80 mL) was introduced into the column using a peristaltic pump at 2 mL/min flowrate. Samples from the column effluent were collected for the determination of IC concentration by UV–Vis spectrometry at 610 nm.

Table 1
Adsorption isotherms for Indigo Carmine on nanosized (nMOS) and bulk adsorbent (bMOS) from *Moringa oleifera* seeds.

Adsorption isotherms	Description	Parameters	Adsorbent	
			nMOS	bMOS
Freundlich	q_e = IC adsorbed in the equilibrium	K_F	2.046	$1.258 \cdot 10^{-1}$
$q_e = K_F C_e^{1/n}$	C_e = IC concentration in the liquid phase in the equilibrium	1/n	1.256	$9.776 \cdot 10^{-1}$
	K_F = volume of the adsorbent	R^2	$9.040 \cdot 10^{-1}$	$8.640 \cdot 10^{-1}$
	1/n = intensity of the analyte adsorption	SE	$4.948 \cdot 10^{-1}$	$6.038 \cdot 10^{-1}$
Langmuir	q_{max} = maximum adsorption capacity	q_{max} (mg/g)	$6.024 \cdot 10^{1}$	$1.400 \cdot 10^{1}$
$q_e = \dfrac{q_{max} \ K_L \ C_e}{1 + K_L \ C_e}$	K_L = constant of Langmuir (free energy of adsorption)	K_L (L/mg)	$3.690 \cdot 10^{-2}$	$4.500 \cdot 10^{-3}$
		R^2	$9.967 \cdot 10^{-1}$	$9.940 \cdot 10^{-1}$
		SE	$6.800 \cdot 10^{-3}$	$5.760 \cdot 10^{-2}$
Temkin	ΔQ = adsorption energy (-ΔH)	Q (J/mol)	$3.705 \cdot 10^{3}$	$2.214 \cdot 10^{3}$
$\theta = \dfrac{RT}{\Delta Q} \ln(K_0 C_e)$	K_0 = constant of Temkin	K_0 (L/mg)	$4.271 \cdot 10^{-1}$	$7.930 \cdot 10^{-2}$
	T = temperature (K)	R^2	$8.640 \cdot 10^{-1}$	$8.740 \cdot 10^{-1}$
	R = universal gas constant	SE	$3.982 \cdot 10^{-1}$	$6.023 \cdot 10^{-1}$
	θ = fractional coverage (q_e/q_{max})			
Fowler–Guggenheim (FG)	W = interaction energy between adsorbed molecules	W (J/mol)	$4.750 \cdot 10^{3}$	$1.611 \cdot 10^{3}$
$K_{FG} C_e = \dfrac{\theta}{1-\theta} \exp\left(\dfrac{2\theta W}{RT}\right)$	K_{FG} = constant of Fowler-Guggenheim	K_{FG} (L/mg)	$3.916 \cdot 10^{1}$	$5.643 \cdot 10^{1}$
		R^2	$9.648 \cdot 10^{-1}$	$7.950 \cdot 10^{-1}$
		SE	$1.869 \cdot 10^{-1}$	$5.580 \cdot 10^{-2}$
Kiselev	K_K = constant of Kiselev	K_K (L/mg)	$3.620 \cdot 10^{-2}$	$8.200 \cdot 10^{-3}$
$K_K C_e = \dfrac{\theta}{(1-\theta)(1+K_n\theta)}$	K_n = complex formation between adsorbed molecules	K_n	$7.458 \cdot 10^{-1}$	$9.024 \cdot 10^{-1}$
		R^2	$5.617 \cdot 10^{-1}$	$6.739 \cdot 10^{-1}$
		SE	$2.141 \cdot 10^{-1}$	$3.440 \cdot 10^{-2}$
Hill–de Boer	K_1 = constant of Hill–de Boer	K_1 (L/mg)	$4.268 \cdot 10^{1}$	$1.401 \cdot 10^{1}$
$K_1 C_e = \dfrac{\theta}{1-\theta} \exp\left(\dfrac{\theta}{1-\theta} - \dfrac{K_2\theta}{RT}\right)$	K_2 = interaction between adsorbed molecules	K_2 (J/mol)	$1.126 \cdot 10^{4}$	$1.963 \cdot 10^{3}$
		R^2	$9.784 \cdot 10^{-1}$	$7.768 \cdot 10^{-1}$
		SE	$1.722 \cdot 10^{-1}$	$7.278 \cdot 10^{-1}$

Table 2

Kinetic model constants, determination coefficients, and standard error of estimate for Indigo Carmine adsorption on nanosized (nMOS) and bulk adsorbent (bMOS) from *Moringa oleifera* seeds.

Adsorption kinetic model	Description	Parameters	Adsorbent	
			nMOS	bMOS
Elovich $q_t = \frac{1}{\beta}\ln(1 + \alpha\beta t)$	q_t = amount of IC adsorbed at time t	α (g/mg min)	$1.220 \cdot 10^{26}$	$4.831 \cdot 10^1$
	β = constant related to the extent of surface coverage	β (mg/g)	2.884	$6.271 \cdot 10^{-1}$
	α = initial adsorbed rate	R^2	$9.332 \cdot 10^{-1}$	$9.479 \cdot 10^{-1}$
		SE	$1.279 \cdot 10^{-1}$	$2.884 \cdot 10^{-1}$
First order $\ln(q_e - q_t) = b - k_1 t$	q_e = amount of IC adsorbed at equilibrium	k_1 (1/min)	$1.340 \cdot 10^{-1}$	$1.360 \cdot 10^{-2}$
	k_1 = apparent adsorption rate coefficient	b	$5.204 \cdot 10^{-1}$	1.546
	b = constant	R^2	$7.445 \cdot 10^{-1}$	$9.371 \cdot 10^{-1}$
		SE	1.195	$3.718 \cdot 10^{-1}$
Parabolic diffusion $q_t = a + k_d t^{1/2}$	k_d = apparent diffusion rate coefficient	k_d (mg/g·min$^{1/2}$)	$2.136 \cdot 10^{-1}$	$8.789 \cdot 10^{-1}$
	a = constant.	a (mg/g)	$2.121 \cdot 10^1$	3.250
		R^2	$7.575 \cdot 10^{-1}$	$8.022 \cdot 10^{-1}$
		SE	$2.437 \cdot 10^{-1}$	1.603
Power function $q_t = k_p C_o t^{1/m}$	k_p = apparent adsorbed rate coefficient	k_p	$2.119 \cdot 10^1$	7.0648
	1/m = model parameter.	1/m	$1.600 \cdot 10^{-2}$	$1.280 \cdot 10^{-1}$
	C_0 = initial concentration of IC	R^2	$9.308 \cdot 10^{-1}$	$9.544 \cdot 10^{-1}$
		SE	$2.600 \cdot 10^{-3}$	$9.300 \cdot 10^{-3}$

2.5. Statistics

In this study, all the experimental data is reported as the mean of the three replicates. Error bars represent the standard error of the mean. Microsoft Excel was used to fit the experimental data to the equation models in Tables 1 and 2 using the linear least squares regression.

3. Results and discussion

3.1. Characterization of adsorbent nanoparticles

The crystalline and amorphous nature of nMOS was analyzed using X-ray diffraction (supplementary material, section 1, Fig. S1). The poorly resolved peaks confirmed the predominance of amorphous materials. Characteristic peaks for decanoic acid, dodecyl-3,5-dinitrobenzate, n-caprylanilide, lauric acid and calciferol were confirmed by the presence of peaks at $2\theta = 3.7°$ and $86.4°$, $22.2°$ and $28.3°$, $42.4°$ and $64.12°$, $50.12°$ and $52.1°$ and, $23.64°$ and $26.27°$, respectively. The abundance of amorphous materials in nMOS due
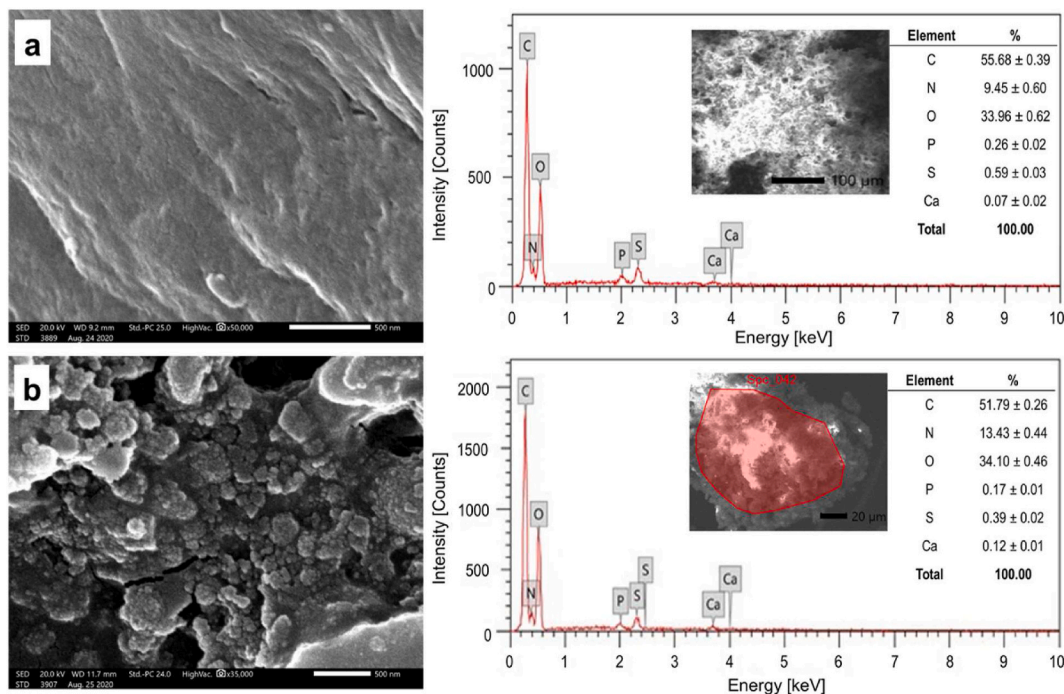

Fig. 1. SEM-EDS analysis of a) bare nMOS and b) nMOS with absorbed Indigo Carmine.

to its lignocellulosic nature was reported in literature by Hamadeen et al. (2021).

The scanning electron microscopy image of nMOS in Fig. 1a reveals a smooth morphology with no breaks on the surface. After IC adsorption on nMOS, some differences were observed in particle structures (Fig. 1b). Numerous pores and nanosized spherical shapes appeared. Different agricultural adsorbents showed similar changes in the surface after the adsorption, as reported by Fernandez et al. (2015) in orange peels and Han et al. (2010) in wheat straw. The EDS analysis was used to identify the elemental composition of nMOS before and after IC adsorption. The results showed high concentrations of carbon (55.68%), oxygen (33.96%), and nitrogen (9.45%) in bare nMOS, whereas other elements showed very low concentration: sulfur (0.59%), phosphorus (0.26%), and calcium (0.07%) (Fig. 1a). The adsorption of IC on nMOS was confirmed by the increased concentrations of nitrogen (13.43%), oxygen (34.10%) and calcium (0.12%) (Fig. 1b). The lower carbon (51.79%), phosphorus (0.17%) and sulfur (0.39%) concentration after the IC adsorption was attributed to the interaction of the absorbent with IC functional groups (Hamadeen et al., 2021).

The transmission electron microscope image of bMOS and nMOS (Supplementary material, section 1, Fig. S2) shows the agglomerated state of nanoparticles and confirmed the nanoscale particle size range (~5.9–26.4 nm). The specific surface area (SSA) of nMOS is 4.6 m^2/g while bMOS has an SSA of 2.6 m^2/g nMOS samples showed ~1.8 times higher SSA than bMOS, which suggest higher adsorption capacity of nMOS.

The FTIR spectrum of bare nMOS (supplementary material, Fig. S4) shows an active band at 3375.5 cm^{-1} that is related to –OH and –NH$_2$ stretching vibration in lignin, proteins, carbohydrates and fatty acids, whereas the band at 2926.5 cm^{-1} is related to the aliphatic C–H group (Feng et al., 2011). The strong peak at 1656.87 cm^{-1} corresponds to the C–O bond of amides or N–H bending in proteins (Arief et al., 2008; Çelekli et al., 2009), whereas the bands at 1540.51 and 1060.19 cm^{-1} can be related to C=O stretch (Chaari et al., 2019; Fernandez et al., 2015). The FTIR spectrum of nMOS after the IC adsorption shows changes in peak intensity and wavenumber (supplementary material, Fig. S4). The changes in wavenumber and peak intensity reveal the interaction of Indigo Carmine with the functional groups of moringa such as –OH bond, C–H group, C–O bonds of amides and N–H groups in carbohydrates, fatty acids and proteins. These functional groups have a main role in the adsorption reaction (Araújo et al., 2010, 2013).

3.2. Adsorption isotherms

Six adsorption isotherms were used to fit the experimental data from the adsorption tests of IC on bMOS and nMOS (Table 1). The higher coefficient of determination (R^2) and the lower standard error (SE) for Langmuir model proved that the IC adsorption by bMOS and nMOS corresponds with a monolayer of adsorbate covering the active centers of the adsorbent surface, as predicted by Langmuir isotherm (Supplementary material, Fig. S5). The Langmuir isotherm was also identified as the adsorption model for other compounds such as methylene blue and crystal violet on adsorbents derived from lignocellulosic materials (Zulfajri et al., 2021). As per Langmuir isotherm, the maximum adsorption capacity (q$_{max}$) was 60.24 mg/g for nMOS and 14.00 mg/g for bMOS. nMOS was 4.3 times more effective than bMOS. This is due to the higher nMOS specific surface area. Compared with literature results (Table 3), nMOS in this study is more effective retaining IC from aqueous solutions than other organic and inorganic materials.

3.3. Optimization of Indigo Carmine adsorption

Contact time is a crucial factor that may define the practical application of the sorbents for large scale applications. The influence of contact time on the adsorption of IC by nMOS was studied at 100 mg/L from 5 min to 24 h. The adsorption of IC on nMOS was very fast during the first 15 min and then, it tended to an equilibrium plateau (Fig. 2). The maximum adsorption capacity of IC on nMOS was reached at 30 min with approximately 93% IC removal from the aqueous solution. The rapid IC adsorption by nMOS in the first 15 min was referred to the availability of vacant active sites in the beginning of the test. As the adsorption process progressed, the adsorption sites have been occupied with the dye molecules and the vacant sites became limited (Alkan et al., 2008; Deniz and Karaman, 2011; Ferreira et al., 2019; Gulnaz et al., 2011). Similar results were reported by Dastgerdi et al. (2019) who needed just 15 min for the complete adsorption of IC on carbon nanotubes. The highly fast IC adsorption on nMOS adsorbent in the beginning of the test could be explained by complex coagulation mechanisms between the adsorbent and adsorbate, as reported by Okuda et al. (2001).

The adsorbent dose affects adsorption results because the increasing availability of surface area and binding sites of the adsorbent. The influence of nMOS adsorbent dose from 100 mg to 400 mg was studied at initial IC concentration of 100 mg/L (Fig. 3). The results showed an increasing IC removal percentage from 93.5% to 98.3% with the adsorbent dose. These results were expected because more IC can be removed from the solution if the vacant sites in the adsorbent increased 4 times (from 100 mg to 400 mg). Conversely, the

Table 3
Adsorption capacity of various absorbents for removal of Indigo Carmine in aqueous effluents.

| Adsorbents	Adsorption capacity (mg/g)	References
Synthesized zeolite ZM	1.2	de Carvalho et al. (2011)
Fly ash	1.5	de Carvalho et al. (2011)
Pistia stratiotes	41.2	Erreira et al. (2019)
PAN/Fe$_3$O$_4$–MPA composite nanofibers	154.5	Yazdi et al. (2018)
Activated sewage sludge	60.0	Otero et al. (2003)
Activated carbonaceous material (tea waste)	20.0	Kesraoui et al. (2017)
Montmorillonite	40.0	Geyikçi (2016)
Mg/Fe layered double hydroxide nanoparticles	55.5	Ahmed and Mohamed (2017)
Moringa oleifera seeds (nanosized adsorbent)	60.2	This work
Moringa oleifera seeds (bulk adsorbent)	14.0	This work
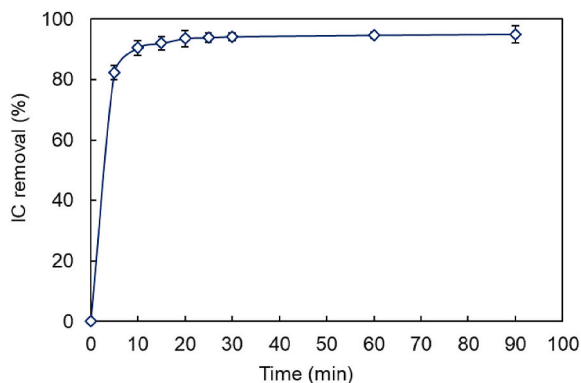
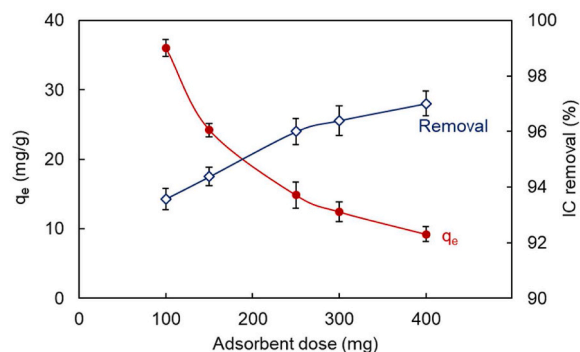**Fig. 2.** Effect of contact time in the adsorption of Indigo Carmine on nMOS.

Fig. 3. Effect of adsorbent dose in the adsorption of Indigo Carmine on nMOS.

adsorption capacity (q_e) decreased with the adsorbent dose. In Fig. 3, adsorbent increased 4 times whereas the amount of IC removed slightly increased. As a result, the sorption capacity decrease due to the limited amount of IC in solution. Some authors (Li et al., 2012; Zhang and Ou, 2017) suggested that the decreasing of the adsorption capacity at higher adsorbent dose could be explained by the decreasing number of active sorption cites and effective specific surface areas due to the agglomeration of the adsorbent nanoparticles at higher doses. However, in our results in Fig. 3, it is evident that the decreasing of q_e is due to the adsorbate/absorbent ratio in each test. Similar results have been reported in dye adsorption on cupuassu shell, *Chara contraria* and chitosan beads (Cardoso et al., 2011; Çelekli et al., 2012, 2011; Morais da Silva et al., 2020).

The pH of the liquid phase is an essential parameter that affects the adsorption process because of its major influence in ionization of adsorbate functional groups and adsorbent surface charge (Das and Jana, 2006; de Oliveira Brito et al., 2010; Verma et al., 2012). In order to explore the impact of dye solution pH in the adsorption process, various tests at different pH in the range of pH 2–11 were carried out. The experimental results showed that the highest removal capacity (93%) of nMOS for IC dye was achieved at pH = 4, and
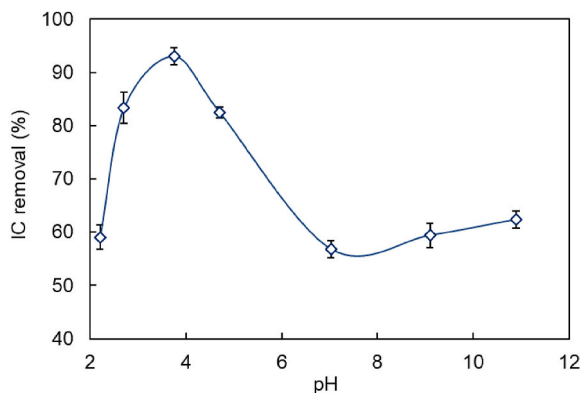

Fig. 4. Effect of solution pH in the adsorption of Indigo Carmine on nMOS.

then the IC removal decreased when the pH increased up to 11 (Fig. 4). These results are consistent with those from Shirani et al. (2018) who reported that the surface of the sorbent (Moringa seeds pods) was positively charged at pH lower than pH_{PZC}, and the positive charge in the surface retained preferently anionic dyes. Thus, the preferred adsorption of IC dye by nMOS at slightly acid conditions can be explained by the $pH_{PZC} = 5$ of nMOS (Supplementary material, Fig. S6). It is well documented that the adsorption of anions is higher when pH < pH_{PZC}, because the adsorbent shows positive charge on the outer surface (Verma et al., 2012) and the adsorbate (anions) are retained by electrostatic attraction. At pH higher than pH_{PZC}, there is an electrostatic repulsion and that decreases the rate and extention of the adsorption (Naveen et al., 2011; Rehman et al., 2014; Yang et al., 2006). Various studies with Indigo Carmine also found that the adsorption was favored at pH below the pH_{PZC} for adsorbents such as *Terminalia catappa* shell modified with broiler egg (Zein et al., 2022), activated carbon from sawdust (Bhowmik et al., 2021), water treatment residuals (El-Kammah et al. 2022) and fish scales biochar (Achieng et al., 2019).

The influence of the IC dye concentrations (10–400 mg/L) was studied using an absorbent dose of 100 mg of nMOS. The results in Fig. 5 showed a significant increase in the adsorption capacity of nMOS and a decline in removal percentage when the initial IC dye concentration increased from 10 to 400 mg/L. This is because the amount of adsorbent remains constant in all the tests, but the amount of IC increases, so, the fraction of adsorbed IC decreases. The results in Fig. 5 showed a saturation of the adsorbent at $q_e = 150$ mg/g in the interval 400–500 mg/L of IC. Initial dye concentration is considered a driving force that stimulates the molecules of IC dye to move from the solution to the adsorbent surface. Several studies have reported similar adsorption behavior (Bhomick et al., 2018; Karaer and Uzun, 2013; Yusuff et al., 2017). Opposite trend for the concentration effect was reported by Kismir and Aroguz (2011) in the adsorption of Brilliant Green on Saklıkent mud, but this was due to the adsorption conditions that were far from the saturation of the adsorbent.

3.4. Adsorption kinetics

The adsorption kinetics of nMOS for IC were studied at different time intervals (Supplementary material, Fig. S7). Adsorption of IC on nMOS was very fast in the first 15 min and then decreased and reached the equilibrium at 30 min with approximately 93% IC removal. The adsorption kinetic data of IC were fitted to four kinetic models (Table 2). Both First order and parabolic diffusion models did not represent the adsorption kinetics as shown by the high SE. Elovich and power function kinetic models showed the highest determination coefficients (R^2) and the lowest SE values. Similar results were reported for removal of different anionic dyes by organo-bentonite as reported by Shen et al. (2009). The IC adsorption rate on nMOS was much faster than that on bMOS as it can be concluded from the kinetic coefficient k_1 of the power function, the model that best represent the adsorption kinetics in nMOS and bMOS.

3.5. Adsorption thermodynamics

The thermodynamic study of the IC adsorption on nMOS was done at 25, 35 and 45 °C. The results showed that temperature decreased the IC adsorption on nMOS from 93.5% to 88.7%. This suggests the exothermic character of the IC sorption (Supplementary material, Figs. S8 and S9). The thermodynamic parameters of IC sorption: Gibbs free energy ($\Delta G°$), enthalpy ($\Delta H°$) and entropy ($\Delta S°$) were determined using equations (3) and (4):

$$\Delta G = - RT \ln K_c \qquad [3]$$

$$\ln K_c = \Delta S°/R - \Delta H°/RT \qquad [4]$$

Where K_c is the equilibrium constant obtained with the Langmuir equation ($K_c = q_e/C_e$ at 298.15–318.15 K), R is the ideal gas constant (8.314 J/mol·K), and T is the temperature in K. The values of $\Delta S°$ and $\Delta H°$ were calculated from the intercept ($\Delta S°/R$) and slope ($\Delta H°/R$) from the plot of ln Kc versus 1/T (Supplementary material, Fig. S8). The negative values of $\Delta G°$ in Table 4 suggest the spontaneity and favorable nature of IC adsorption on nMOS (Ho et al., 2000; Li et al., 2018). The $\Delta G°$ values are more negative with the temperature showing the favorable thermodynamics of IC adsorption on nMOS at higher temperatures. The negative magnitude of enthalpy change ($\Delta H°$) confirmed that the IC adsorption process is exothermic. Similar results were obtained from the thermodynamic study of basic yellow 2 and Safranin-O dyes adsorption on poplar leaf and acid treated coconut coir (Aghdasinia et al., 2021; Ghosh
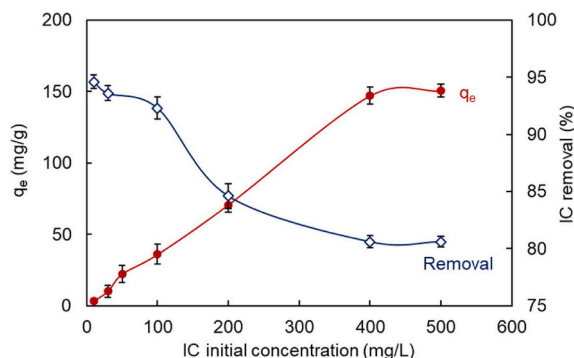

Fig. 5. Effect of initial Indigo Carmine concentration in the adsorption on nMOS.

Table 4

Thermodynamic parameters for Indigo Carmine (IC) adsorption on nanosized adsorbent (nMOS).

Adsorbent	Initial IC concentration (mg/L)	T (K)	$\Delta G°$ (kJ/mol)	$\Delta S°$ (kJ/mol K)	$\Delta H°$ (kJ/mol)
nMOS	30	298.15	−4366.70	65.95	−2398
		308.15	−3639.80		
		318.15	−3047.60		
	100	298.15	−2061.20	96.61	−30625
		308.15	−415.54		
		318.15	−128.99		

et al., 2021). The positive values of entropy $\Delta S°$ indicate a randomness decrease at the solid/solution interface with no significant variations in the internal structure of the adsorbent.

3.6. Proposed mechanism of adsorption

The major proposed interactions between IC and nMOS are presented in Fig. 6 and include: (1) hydrogen bonding, (2) electrostatic interactions, and (3) π-π interaction.

Hydrogen bonding interaction (1): The nMOS sorbent contains –OH groups whereas IC dye contains O (strong H donors). The hydrogen bond is proposed to occur between the IC strong H donor (O) and nMOS H acceptor (-OH). The FTIR spectra of nMOS after IC adsorption confirmed the involvement of –OH groups of nMOS in the retention of IC. Li et al. (2018) reported the participation of H bond in the adsorption process of IC dye by nanofiber membranes.

Electrostatic interactions (2): The negatively charged molecules of the anionic IC dye interact with the positively charged adsorbent functional groups on the surface (i.e. under acidic conditions, when pH < pH$_{PZC}$, the –OH on the adsorbent surface could be protonated with H$^+$ to produce –OH$_2^+$). Therefore, the electrostatic interactions between the protonated hydroxyl groups of nMOS and SO$_3^-$ groups of the IC dye, probably contribute to IC adsorption.

The π–π interaction (3): nMOS surface is quite rich on π electron (i.e., O$_2$ molecules on the surface of nMOS act as electron donors). Thus, the π–π interaction could possibly take place between π electrons on nMOS surface and the π electron cloud of IC benzene ring.

The proposed mechanisms in this study are compatible with the mechanisms proposed by Beltrán-Heredia et al. (2009) for the adsorption of various dyes (inclidng IC) on Moringa oleifera seeds. El-Kammah et al. (2022) also described the three interactions (hydrogen bonding, electrostatic, and π-π interactions) in the adsorption of IC on water treatment residuals (WTR), a waste from dirnking water plants. Gomes et al. (2022) summarize the studies from the last decade using *Moringa oleifera* as adsorbent. The mian mechanisms of adsorbent-adsorbate interactions include electrostatic interaction, hydrogen bonds, and van der Waals forces, varying in relative importance depending on the chemical or physical nature of adsorption.

3.7. Adsorption/desorption and reusability of nMOS

Reusability of nMOS is an important aspect for economic and practical application of the adsorption process. Thus, sequential batch adsorption-desorption tests were performed to assess nMOS reusability. Tests were done in triplicate mixing 0.1 g nMOS with 20 mL of IC dye solution, and shaking the suspension for 30 min. The mixture was centrifuged and IC was determined in the supernatant solution. After discarding the supernatant solution, IC was desorbed form the adsorbent adding 20 mL of deionized water. This process was repeated 5 times and the results are pltted in Fig. 7. The experimental results showed that the IC adsorption slightly decreased from the first (93%) to the fourth (82%) cycle. In the fifth cycle, the IC removal was only 75% suggesting an irreversible loss of adsorption capacity.

3.8. Textile wastewater treated with nMOS

The potential of nMOS as a practical adsorbent for IC was tested with real textile wastewater. Samples of textile wastewater contaminated with IC were collected from a textile and spinning company at Kafr El-Dawar (Elboheira governorate, Egypt). The samples were filtered (Whatman cellulose filter paper) to remove suspended solid and other impurities. The chemical characteristics of the textile wastewater are reported in Table 5. The concentration of IC in the textile effluent was 43.65 mg/L. Pure IC solutions with a concentration of 50 mg/L were prepared in the laboratory. The adsorption tests with both samples: textile wastewater and IC pure solutions were conducted in batch and packed-bed columns. The IC removal from textile wastewater was 85.6% in batch tests and 84% in packed-bed column. In the test with IC pure solutions, the removal was 91.63% in batch tests and 90.32% in packed-bed column tests (Supplementary material, Fig. S10). These results proved the capacity of nMOS as absorbent for IC even in real textile effluents. Similar results were found in the adsorption of IC in textile effluents on nanosized adsorbent derived from WTR (water treatment residuals), a waste from drinking water treatment plants (El-Kammah et al., 2022a). The slightly lower removal in textile wastewater can be explained for the presence of salts and other contaminants that may exert some competing effects in the active centers of the adsorbent surface. Besides, the high ionic concentration in the textile wastewater may have a significant influence in the physico-chemical conditions in the surface of the adsorbent that may limit the interaction between adsorbate and adsorbent.

4. Conclusions

In this study, we have prepared an adsorbent material at the nanoscale using the waste from the oil extraction from *Moringa oleifera* seeds. Nanoparticles from *Moringa oleifera* seeds, nMOS, were characterized and tested for the adsorption of Indigo Carmine. The
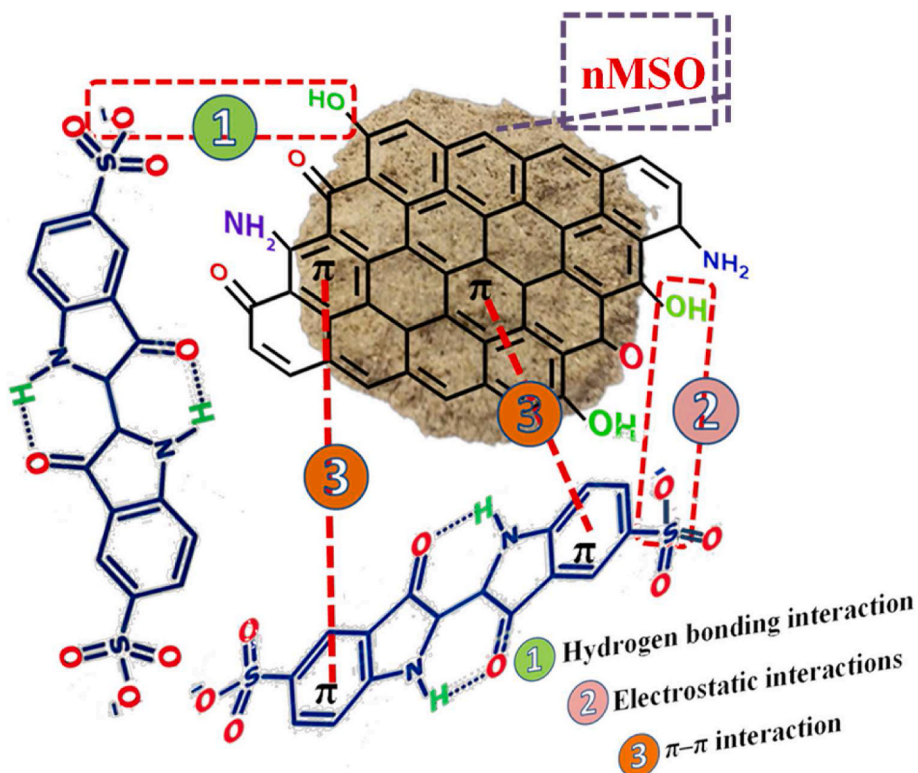
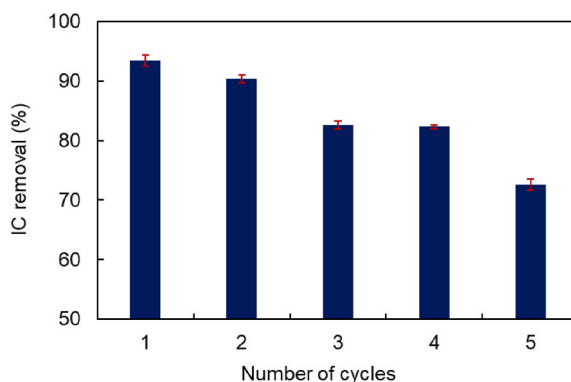**Fig. 6.** Suggested mechanisms for Indigo Carmine adsorption on nMOS.

Fig. 7. Adsorption of Indigo Carmine on nMOS after five adsorption-desorption cycles.

results were compared with the bulk material, bMOS. The maximum adsorption capacity of nMOS was 60.24 mg/g, which is 4.3 times higher than that of bMOS. IC adsorption was modeled with Langmuir isotherm and power function kinetic model. The thermodynamic analysis confirmed that the adsorption is spontaneous ($\Delta G° < 0$) and exothermic. The adsorption was favored with temperature. The possible mechanisms of IC adsorption on nMOS involved π-π electron interaction, hydrogen bridge bond and electrostatic interaction between adsorbent and adsorbate. nMOS can be reused in successive adsorption/desorpción cycles with minimum loss of activity, at least for 4 cycles. The favorable adsorption with pure IC solutions was also confirmed with textile wastewater contaminated with similar concentration of IC.

This study have proved that nMOS is a promising adsorbent material with potential use in the treatment of textile wastewater. Further studies at large scale are needed to verify the real behavior of nMOS in industrial conditions. It is also necessary to assess the nMOS performance with effluents containing multiple pollutants.

Table 5
Chemical characterization of textile wastewater effluent.

Analyte	Units	Values	Analyte	Units	Values
pH	-	7.32	IC	mg/L	43.65
EC	dS/m	1.20	Ca^{2+}	meq/L	2.70
TDS	mg/L	847	Mg^{2+}	meq/L	2.27
SAR	-	4.58	Na^{2+}	meq/L	7.22
Cd^{2+}	mg/L	0.02	K^+	meq/L	0.41
Zn^{2+}	mg/L	0.86	CO_3^{2-}	meq/L	0.00
Ni^{2+}	mg/L	0.19	HCO_3^-	meq/L	2.35
Pb^{2+}	mg/L	0.34	Cl^-	meq/L	5.52
Co^{2+}	mg/L	0.03	SO_4^{2-}	meq/L	4.42

EC: Electric Conductivity.
TDS: Total Dissolved Salts.
IC: Indigo Carmine dye.

SAR: Sodium Adsorption Ratio, $SAR = \dfrac{Na^+}{\sqrt{\dfrac{Ca^{2+} + Mg^{2+}}{2}}}$

CRediT authorship contribution statement

Mai El-Kammah: Investigation, Methodology, Analysis, and Writing-original draft. **Elsayed Elkhatib:** Conceptualization, Supervision, Validation, Writing-Reviewing and Editing. **Susana Gouveia:** Supervision, Methodology, Analysis, Review and Editing. **Claudio Cameselle:** Supervision, Methodology, Analysis, Review and Editing. **Emad Aboukila:** Supervision, Data Curation, Validation, Review and Editing.

Declaration of competing interest

The authors declare that they have no known competing financial interests or personal relationships that could have appeared to influence the work reported in this paper.

Appendix A. Supplementary data

Supplementary data to this article can be found online at https://doi.org/10.1016/j.scp.2022.100753.

References

Achieng, G.O., Kowenje, C.O., Lalah, J.O., Ojwach, S.O., 2019. Preparation, characterization of fish scales biochar and their applications in the removal of anionic indigo carmine dye from aqueous solutions. Water Sci. Technol. 80 (11), 2218–2231.

Afroze, S., Sen, T.K., 2018. A review on heavy metal ions and dye adsorption from water by agricultural solid waste adsorbents. Water Air Soil Pollut. 229 (7), 1–50.

Agbahoungbata, M.Y., Fatombi, J.K., Ayedoun, M.A., Idohou, E., Sagbo, E.V., Osseni, S.A., Aminou, T., 2016. Removal of reactive dyes from their aqueous solutions using Moringa oleifera seeds and Grewia venusta peel. Desalination Water Treat. 57 (47), 22609–22617.

Aghdasinia, H., Gholizadeh, M., Hosseini, S.S., 2021. Adsorptive removal of basic yellow 2 onto reed stem and poplar leaf: a comprehensive study. Sustain. Chem. Pharm. 24, 100546.

Ahmed, M.A., Mohamed, A.A., 2017. An efficient adsorption of indigo carmine dye from aqueous solution on mesoporous Mg/Fe layered double hydroxide nanoparticles prepared by controlled sol-gel route. Chemosphere 174, 280–288.

Alkan, M., Doğan, M., Turhan, Y., Demirbaş, Ö., Turan, P., 2008. Adsorption kinetics and mechanism of maxilon blue 5G dye on sepiolite from aqueous solutions. Chem. Eng. J. 139, 213–223.

Anwar, F., Ashraf, M., Bhanger, M.I., 2005. Interprovenance variation in the composition of Moringa oleifera oilseeds from Pakistan. J. Am. Oil Chem. Soc. 82, 45–51.

Araújo, C.S.T., Carvalho, D.C., Rezende, H.C., Almeida, I.L.S., Coelho, L.M., Coelho, N.M.M., Marques, T.L., Alves, V.N., 2013. Bioremediation of waters contaminated with heavy metals using Moringa oleifera seeds as biosorbent. Appl. Bioremed.-Active Passive Approach. 23, 227–255.

Araújo, C.S.T., Melo, E.I., Alves, V.N., Coelho, N.M.M., 2010. Moringa oleifera Lam. seeds as a natural solid adsorbent for removal of AgI in aqueous solutions. J. Braz. Chem. Soc. 21, 1727–1732.

Arief, V.O., Trilestari, K., Sunarso, J., Indraswati, N., Ismadji, S., 2008. Recent progress on biosorption of heavy metals from liquids using low cost biosorbents: characterization, biosorption parameters and mechanism studies. Clean: Soil, Air, Water 36, 937–962.

Behera, M., Nayak, J., Banerjee, S., Chakrabortty, S., Tripathy, S.K., 2021. A review on the treatment of textile industry waste effluents towards the development of efficient mitigation strategy: an integrated system design approach. J. Environ. Chem. Eng. 9 (4), 105277.

Beltrán-Heredia, J., Sánchez-Martín, J., Delgado-Regalado, A., 2009. Removal of carmine indigo dye with Moringa oleifera seed extract. Ind. Eng. Chem. Res. 48 (14), 6512–6520.

Bhomick, P.C., Supong, A., Baruah, M., Pongener, C., Sinha, D., 2018. Pine Cone biomass as an efficient precursor for the synthesis of activated biocarbon for adsorption of anionic dye from aqueous solution: isotherm, kinetic, thermodynamic and regeneration studies. Sustain. Chem. Pharm. 10, 41–49. https://doi.org/10.1016/j.scp.2018.09.001.

Bhowmik, S., Chakraborty, V., Das, P., 2021. Batch adsorption of indigo carmine on activated carbon prepared from sawdust: a comparative study and optimization of operating conditions using Response Surface Methodology. Result Surf. Interf. 3, 100011.

Cameselle, C., Reddy, K.R., 2019. Elemental iron and other nanotechnologies for soil remediation. In: Engineering Tools for Environmental Risk Management–4: Risk Reduction Technologies and Case Studies. CRC Press, pp. 465–495.

Cardoso, N.F., Lima, E.C., Pinto, I.S., Amavisca, C.V., Royer, B., Pinto, R.B., Alencar, W.S., Pereira, S.F.P., 2011. Application of cupuassu shell as biosorbent for the removal of textile dyes from aqueous solution. J. Environ. Manag. 92, 1237–1247.

Çelekli, A., İlgün, G., Bozkurt, H., 2012. Sorption equilibrium, kinetic, thermodynamic, and desorption studies of Reactive Red 120 on Chara contraria. Chem. Eng. J. 191, 228–235.

Çelekli, A., Tanrıverdi, B., Bozkurt, H., 2011. Predictive modeling of removal of Lanaset Red G on Chara contraria; kinetic, equilibrium, and thermodynamic studies. Chem. Eng. J. 169, 166–172.

Çelekli, A., Yavuzatmaca, M., Bozkurt, H., 2009. Kinetic and equilibrium studies on the adsorption of reactive red 120 from aqueous solution on Spirogyra majuscula. Chem. Eng. J. 152, 139–145.

Chaari, I., Fakhfakh, E., Medhioub, M., Jamoussi, F., 2019. Comparative study on adsorption of cationic and anionic dyes by smectite rich natural clays. J. Mol. Struct. 1179, 672–677.

Choi, K.Y., 2021. Discoloration of indigo dyes by eco-friendly biocatalysts. Dyes Pigments 184, 108749.

Chowdhury, M.F., Khandaker, S., Sarker, F., Islam, A., Rahman, M.T., Awual, M.R., 2020. Current treatment technologies and mechanisms for removal of indigo carmine dyes from wastewater: a review. J. Mol. Liq. 318, 114061.

Das, N., Jana, R.K., 2006. Adsorption of some bivalent heavy metal ions from aqueous solutions by manganese nodule leached residues. J. Colloid Interface Sci. 293, 253–262.

Dastgerdi, Z.H., Meshkat, S.S., Esrafili, M.D., 2019. Enhanced adsorptive removal of Indigo carmine dye performance by functionalized carbon nanotubes based adsorbents from aqueous solution: equilibrium, kinetic, and DFT study. J. Nanostruct. Chem. 9, 323–334.

Davies, G., McGregor, J., 2021. Hydrothermal synthesis of biomass-derived magnetic carbon composites for adsorption and catalysis. ACS Omega 6 (48), 33000–33009.

de Carvalho, T., Fungaro, D., Magdalena, C., Cunico, P., 2011. Adsorption of indigo carmine from aqueous solution using coal fly ash and zeolite from fly ash. J. Radioanal. Nucl. Chem. 289, 617–626.

de Oliveira Brito, S.M., Andrade, H.M.C., Soares, L.F., de Azevedo, R.P., 2010. Brazil nut shells as a new biosorbent to remove methylene blue and indigo carmine from aqueous solutions. J. Hazard Mater. 174, 84–92.

Deniz, F., Karaman, S., 2011. Removal of Basic Red 46 dye from aqueous solution by pine tree leaves. Chem. Eng. J. 170, 67–74.

Donkadokula, N.Y., Kola, A.K., Naz, I., Saroj, D., 2020. A review on advanced physico-chemical and biological textile dye wastewater treatment techniques. Rev. Environ. Sci. Biotechnol. 19 (3), 543–560.

Du, J., Wu, Y., Dong, Z., Zhang, M., Yang, X., Xiong, H., Zhao, L., 2022. Single and competitive adsorption between Indigo Carmine and Methyl orange dyes on quaternized kapok fiber adsorbent prepared by radiation technique. Separ. Purif. Technol. 292, 121103.

Edwin, D.S.S., Manjunatha, J.G., Raril, C., Girish, T., Ravishankar, D.K., Arpitha, H.J., 2021. Electrochemical analysis of indigo carmine using polyarginine modified carbon paste electrode. J. Electrochem. Sci. Eng. 11 (2), 87–96.

El-Kammah, M., Elkhatib, E., Gouveia, S., Cameselle, C., Aboukila, E., 2022a. Cost-effective ecofriendly nanoparticles for rapid and efficient indigo carmine dye removal from wastewater: adsorption equilibrium, kinetics and mechanism. Environ. Technol. Innovat. 28, 102595.

El-Kammah, M., Elkhatib, E., Gouveia, S., Cameselle, C., Aboukila, E., 2022b. Enhanced removal of Thiamethoxam from wastewater using waste-derived nanoparticles: adsorption performance and mechanisms. Environ. Technol. Innovat. 28, 102713.

Elkhatib, E., Moharem, M., Mahdy, A., Mesalem, M., 2017. Sorption, release and forms of mercury in contaminated soils stabilized with water treatment residual nanoparticles. Land Degrad. Dev. 28, 752–761.

Elkhatib, E.A., Mahdy, A.M., Salama, K.A., 2015. Green synthesis of nanoparticles by milling residues of water treatment. Environ. Chem. Lett. 13, 333–339.

Ferreira, R.M., de Oliveira, N.M., Lima, L.L.S., Campista, A.L.D.M., Stapelfeldt, D.M.A., 2019. Adsorption of indigo carmine on Pistia stratiotes dry biomass chemically modified. Environ. Sci. Pollut. Res. 28614–28621.

Feng, N., Guo, X., Liang, S., Zhu, Y., Liu, J., 2011. Biosorption of heavy metals from aqueous solutions by chemically modified orange peel. J. Hazard Mater. 185, 49–54.

Fernandez, M.E., Ledesma, B., Román, S., Bonelli, P.R., Cukierman, A.L., 2015. Development and characterization of activated hydrochars from orange peels as potential adsorbents for emerging organic contaminants. Bioresour. Technol. 183, 221–228.

Geyikçi, F., 2016. Factorial design analysis for adsorption of Indigo Carmine onto Montmorillonite-Evaluation of the kinetics and equilibrium data. Prog. Org. Coating 98, 28–34.

Ghosh, I., Kar, S., Chatterjee, T., Bar, N., Das, S.K., 2021. Adsorptive removal of Safranin-O dye from aqueous medium using coconut coir and its acid-treated forms: adsorption study, scale-up design, MPR and GA-ANN modeling. Sustain. Chem. Pharm. 19, 100374 https://doi.org/10.1016/j.scp.2021.100374.

Gokul Eswaran, S., Shahid Afridi, P., Vasimalai, N., 2022. Effective multi toxic dyes degradation using bio-fabricated silver nanoparticles as a green catalyst. Appl. Biochem. Biotechnol. 1–16.

Gomes, H.D.O., Paulo de Tarso, C.F., do Nascimento, R.F., Teixeira, R.N.P., 2022. Removal of contaminants from water using Moringa oleifera Lam. as biosorbent: an overview of the last decade. J. Water Proc. Eng. 46, 102576.

Gulnaz, O., Sahmurova, A., Kama, S., 2011. Removal of reactive red 198 from aqueous solution by potamogeton crispus. Chem. Eng. J. 174, 579–585.

Hamadeen, H.M., Elkhatib, E.A., Badawy, M.E.I., Abdelgaleil, S.A.M., 2021. Green low cost nanomaterial produced from Moringa oleifera seed waste for enhanced removal of chlorpyrifos from wastewater: mechanism and sorption studies. J. Environ. Chem. Eng. 9, 105376.

Han, R., Zhang, Lijun, Song, C., Zhang, M., Zhu, H., Zhang, LiJuan, 2010. Characterization of modified wheat straw, kinetic and equilibrium study about copper ion and methylene blue adsorption in batch mode. Carbohydr. Polym. 79, 1140–1149.

Ho, Y.S., Ng, J.C.Y., McKay, G., 2000. Kinetics of pollutant sorption by biosorbents. Separ. Purif. Methods 29, 189–232.

Karaer, H., Uzun, I., 2013. Adsorption of basic dyestuffs from aqueous solution by modified chitosan. Desalination Water Treat. 51, 2294–2305.

Kesraoui, A., Selmi, T., Seffen, M., Brouers, F., 2017. Influence of alternating current on the adsorption of indigo carmine. Environ. Sci. Pollut. Res. 24, 9940–9950.

Kismir, Y., Aroguz, A.Z., 2011. Adsorption characteristics of the hazardous dye Brilliant Green on Saklıkent mud. Chem. Eng. J. 172, 199–206.

Kosmulski, M., 2009. pH-dependent surface charging and points of zero charge. IV. Update and new approach. J. Colloid Interface Sci. 337, 439–448.

Li, C., Lou, T., Yan, X., Long, Y., Cui, G., Wang, X., 2018. Fabrication of pure chitosan nanofibrous membranes as effective absorbent for dye removal. Int. J. Biol. Macromol. 106, 768–774.

Li, M., Wang, H., Wu, S., Li, F., Zhi, P., 2012. Adsorption of hazardous dyes indigo carmine and acid red on nanofiber membranes. RSC Adv. 2, 900–907.

Morais da Silva, P.M., Camparotto, N.G., Figueiredo Neves, T. de, Grego Lira, K.T., Mastelaro, V.R., Siqueira Franco Picone, C., Prediger, P., 2020. Effective removal of basic dye onto sustainable chitosan beads: batch and fixed-bed column adsorption, beads stability and mechanism. Sustain. Chem. Pharm. 18, 100348.

Naveen, N., Saravanan, P., Baskar, G., Renganathan, S., 2011. Equilibrium and kinetic modeling on the removal of Reactive Red 120 using positively charged Hydrilla verticillata. J. Taiwan Inst. Chem. Eng. 42, 463–469.

Okuda, T., Baes, A.U., Nishijima, W., Okada, M., 2001. Coagulation mechanism of salt solution-extracted active component in Moringa oleifera seeds. Water Res. 35, 830–834.

Otero, M., Rozada, F., Calvo, L.F., Garcıa, A.I., Moran, A., 2003. Elimination of organic water pollutants using adsorbents obtained from sewage sludge. Dyes Pigments 57, 55–65.

Ramos, M.D.N., Lima, J.P.P., de Aquino, S.F., Aguiar, A., 2021. A critical analysis of the alternative treatments applied to effluents from Brazilian textile industries. J. Water Proc. Eng. 43, 102273.

Rehman, R., Zafar, J., Nisar, H., 2014. Adsorption studies of removal of indigo caramine dye from water by formaldehyde and urea treated cellulosic waste of citrus reticulata peels. Asian J. Chem. 26, 43–47.

Shen, D., Fan, J., Zhou, W., Gao, B., Yue, Q., Kang, Q., 2009. Adsorption kinetics and isotherm of anionic dyes onto organo-bentonite from single and multisolute systems. J. Hazard Mater. 172, 99–107.

Shirani, Z., Santhosh, C., Iqbal, J., Bhatnagar, A., 2018. Waste Moringa oleifera seed pods as green sorbent for efficient removal of toxic aquatic pollutants. J. Environ. Manag. 227, 95–106.

Sikdar, D., Goswami, S., Das, P., 2020. Activated carbonaceous materials from tea waste and its removal capacity of indigo carmine present in solution: synthesis, batch and optimization study. Sustain. Environ. Res. 30, 1–16.

Tabti, S., Benchettara, A., Smaili, F., Benchettara, A., Berrabah, S.E., 2022. Electrodeposition of lead dioxide on Fe electrode: application to the degradation of Indigo Carmine dye. J. Appl. Electrochem. 1–11.

Verma, A.K., Dash, R.R., Bhunia, P., 2012. A review on chemical coagulation/flocculation technologies for removal of colour from textile wastewaters. J. Environ. Manag. 93, 154–168.

Wakkel, M., Khiari, B., Zagrouba, F., 2019. Textile wastewater treatment by agro-industrial waste: equilibrium modelling, thermodynamics and mass transfer mechanisms of cationic dyes adsorption onto low-cost lignocellulosic adsorbent. J. Taiwan Inst. Chem. Eng. 96, 439–452.

Yang, Y., Zhao, Y.Q., Babatunde, A.O., Wang, L., Ren, Y.X., Han, Y., 2006. Characteristics and mechanisms of phosphate adsorption on dewatered alum sludge. Separ. Purif. Technol. 51, 193–200.

Yazdi, M.G., Ivanic, M., Mohamed, A., Uheida, A., 2018. Surface modified composite nanofibers for the removal of indigo carmine dye from polluted water. RSC Adv. 8, 24588–24598.

Yusuff, S.M., Ong, K.K., Yunus, W., Fitrianto, A., Ahmad, M.B., 2017. Removal of methylene blue from aqueous solutions using alum sludge: sorption optimization by response surface methodology. J. Fund. Appl. Sci. 9, 532–545.

Zein, R., Hevira, L., Fauzia, S., Ighalo, J.O., 2022. The Improvement of Indigo Carmine Dye Adsorption by Terminalia catappa Shell Modified with Broiler Egg White. Biomass Conversion and Biorefinery, pp. 1–18.

Zhang, Y., Ou, D., 2017. Comparison of the removal and adsorption mechanisms of cadmium and lead from aqueous solution by activated carbons prepared from Typha angustifolia and Salix matsudana. RSC Adv. 7, 16092–16103.

Zulfajri, M., Kao, Y.-T., Huang, G.G., 2021. Retrieve of residual waste of carbon dots derived from straw mushroom as a hydrochar for the removal of organic dyes from aqueous solutions. Sustain. Chem. Pharm. 22, 100469.